

Spatial carrier phase-shifting algorithm based on least-squares iteration

Jiancheng Xu,^{1,2,*} Qiao Xu,^{1,2} and Hansheng Peng²

¹Chengdu Fine Optical Engineering Research Center, No. 3 Keyuan 1st Road, Gaoxin, Chengdu, Sichuan, 610041, China

²Laser Fusion Research Center, Chinese Academy of Engineering and Physics, P.O. Box 919-988, Mianyang, 621900, China

*Corresponding author: xujiancheng@ustc.edu

Received 9 May 2008; revised 4 September 2008; accepted 8 September 2008;
posted 9 September 2008 (Doc. ID 95785); published 8 October 2008

An advanced spatial carrier phase-shifting (SCPS) algorithm based on least-squares iteration is proposed to extract the phase distribution from a single spatial carrier interferogram. The proposed algorithm divides the spatial carrier interferogram into four phase-shifted interferograms. By compensating for the effects of the variations of phase shifts between pixels and the variations of background and contrast, the proposed algorithm determines the local phase shifts and phase distribution simultaneously and accurately. Numerical simulations show that the accuracy of the proposed algorithm is obviously improved by compensating for the effects of background and contrast variations. The peak to valley of the residual phase error remains less than 0.002 rad when the magnitude of spatial carrier is in the range from $\pi/5$ to $\pi/2$ and the direction of the spatial carrier is in the range from 25° to 65° . Numerical simulations and experiments demonstrate that the proposed algorithm exhibits higher precision than the existing SCPS algorithms. The proposed algorithm is sensitive to random noise, but the error can be reduced by \sqrt{N} times if N measurements are taken and averaged. © 2008 Optical Society of America

OCIS codes: 120.3180, 120.5050, 120.2650, 050.5080.

1. Introduction

Phase measurement methods are widely used in optical metrology. The two primary groups of fringe pattern analysis techniques are temporal phase measurement (sometimes known as the phase-shifting method) and spatial phase measurement (which is also called the spatial carrier method). Temporal phase measurement [1] is a well-established method for measuring the optical wavefront phase. However, three or more intensity profiles are needed in this technique, and thus it is sensitive to vibration and turbulence. The primary advantage of the spatial phase measurement technique over the temporal phase measurement is that only one image is required. This allows measurements to be taken in adverse conditions or dynamic events. Two popular spatial phase measurement algorithms that we

can mention are the Fourier transform method [2] and spatial carrier phase-shifting (SCPS) method [3]. However, the Fourier transform method is a global operation with a poor spatial localization; thus it cannot extract the characteristics of spatial localization. Furthermore, a large residual phase errors usually appears at the points near the boundaries because of Gibbs effects.

The SCPS is a spatial domain processing technique and is a direct application of a temporal phase-shifting algorithm to spatial phase measurement. It has the unique advantage of retrieving the phase from a single carrier fringe pattern with spatial resolution approaching that of temporal phase measurement. However, this method usually assumes that the phase difference between pixels remains constant over a small interval and is equal to the fringe carrier frequency [4], which results in the largest source of error in this method. Because the phase shift between pixels is a result of both the spatial carrier phase and the test wavefront phase, the

0003-6935/08/295446-08\$15.00/0
© 2008 Optical Society of America

assumption of constant phase shift is valid only for wavefronts with small deviations. The resulting error is analogous to the phase shift calibration error in temporal phase shifting. On the other hand, most of the existing SCPS algorithms require a proper carrier frequency, such as $\pi/2$ rad per pixel [5]; otherwise, residual phase errors will be produced.

In order to solve these problems, Servin and Cuevas [6] presented a solution to eliminate the carrier-frequency leakage problem that was derived as a consequence of presuming a constant phase value over three consecutive pixels. But their solution still assumes that the slope of the detected phase is constant over the pixels in an interval.

Guo *et al.* [7] presented a local frequency estimation approach for the fringe pattern with spatial carrier, by which the 2D spatial frequencies at a certain pixel are estimated from its neighborhood and then the phase distribution is calculated by least-squares method. However, it is hard to determine the size of the neighborhood and it may lose its spatial resolution because of average operation. On the other hand, Styk and Patorski [8] have pointed out the errors caused by the variations of background and contrast, but they did not solve the problem.

In this paper, we present a spatial carrier phase-shifting algorithm based on least-squares iteration to extract the phase from a single interferogram with a spatial carrier. During the iteration, we compensate for the effects of the variations of phase shifts between pixels and the variations of background and contrast; therefore, phase distribution can be obtained with higher accuracy.

2. Theory and Method

A. Transformation from Spatial Carrier Interferogram to Four Phase-Shifting Interferograms

The fringe pattern with a linear spatial carrier is usually represented with

$$I(x,y) = A(x,y) + B(x,y) \cos[\varphi(x,y) + u_c x + v_c y], \quad (1)$$

where $I(x,y)$, $A(x,y)$, and $B(x,y)$ denote the recorded intensity, the background, and the contrast at the location (x,y) , respectively. In Eq. (1) u_c and v_c denote the carrier frequencies along the x and y directions, respectively, and $\varphi(x,y)$ is the phase to be measured. We define that $\Phi(x,y) = \varphi(x,y) + u_c x + v_c y$. Along the two directions, the local frequencies,

$$u(x,y) = \partial[\Phi(x,y)]/\partial x = \partial\varphi(x,y)/\partial x + u_c, \quad (2)$$

$$v(x,y) = \partial[\Phi(x,y)]/\partial y = \partial\varphi(x,y)/\partial y + v_c, \quad (3)$$

respectively, deviate from the carrier frequencies, and the deviations depend on how steep the phase varies. Having four consecutive pixels of the spatial carrier interferogram, we obtain four intensities given by

$$I_1(x,y) = I(x,y) = A_1 + B_1 \cos[\Phi(x,y)], \quad (4)$$

$$I_2(x,y) = I(x+1,y) = A_2 + B_2 \cos[\Phi(x,y) + u(x,y)], \quad (5)$$

$$I_3(x,y) = I(x,y+1) = A_3 + B_3 \cos[\Phi(x,y) + v(x,y)], \quad (6)$$

$$I_4(x,y) = I(x+1,y+1) = A_4 + B_4 \cos[\Phi(x,y) + u(x,y) + v(x,y)], \quad (7)$$

where $A_1 = A(x,y)$, $A_2 = A(x+1,y)$, $A_3 = A(x,y+1)$, and $A_4 = A(x+1,y+1)$; $B_1 = B(x,y)$, $B_2 = B(x+1,y)$, $B_3 = B(x,y+1)$, and $B_4 = B(x+1,y+1)$. If $A(x,y) \approx A_n(x,y)$ and $B(x,y) \approx B_n(x,y)$ ($n = 2, 3, 4$) are satisfied, we can transform the spatial carrier interferogram I into four temporal phase-shifting interferograms, I_1 , I_2 , I_3 , and I_4 . Their relative phase shifts at pixel (x,y) are 0, $u(x,y)$, $v(x,y)$, and $u(x,y) + v(x,y)$, respectively.

B. Iterative Algorithm Determination Phase from Phase Shifts

As in the conventional phase-shifting algorithm [9], we define a new set of variables as $a_n(x,y) = A_n(x,y)$, $b_n(x,y) = B_n(x,y) \cos(\Phi(x,y))$, and $c_n(x,y) = -B_n(x,y) \sin(\Phi(x,y))$. We also define the relative phase shifts at pixel (x,y) as $\theta_n(x,y)$ ($n = 1, 2, 3, 4$), where $\theta_1(x,y) = 0$, $\theta_2(x,y) = u(x,y)$, $\theta_3(x,y) = v(x,y)$ and $\theta_4(x,y) = u(x,y) + v(x,y)$. Then Eqs. (4)–(7) are rewritten as

$$\begin{aligned} & I_n(x,y) - A_n(x,y) + A_1(x,y) \\ &= a_1(x,y) + b_1(x,y) \frac{B_n(x,y)}{B_1(x,y)} \cos[\theta_n(x,y)] \\ &+ c_1(x,y) \frac{B_n(x,y)}{B_1(x,y)} \sin[\theta_n(x,y)]. \end{aligned} \quad (8)$$

For the pixel (x,y) , if $A_n(x,y) - A_1(x,y)$, $B_n(x,y)/B_1(x,y)$, and $\theta_n(x,y)$ are known (we set $A_n(x,y) = A_1(x,y)$ and $B_n(x,y) = B_1(x,y)$ and estimate initial $\theta_n(x,y)$ according to the number of fringes for the first iteration cycle), there are three unknowns and four equations. The unknowns can be solved by use of the least-squares method [9]. The least-squares error between theoretical and experimental interferogram $S(x,y)$, which is accumulated from all the images described by Eq. (8), can be written as

$$S(x,y) = \sum_{n=1}^N [I_n^e(x,y) - I_n(x,y)]^2, \quad (9)$$

where $I_n^e(x,y)$ is the experimentally measured intensity of the interferogram and N denotes the number

of images ($N = 4$). The least-squares criteria required for three unknowns ($a_1(x,y)$, $b_1(x,y)$, and $c_1(x,y)$) can be expressed as

$$\frac{\partial S(x,y)}{\partial a_1(x,y)} = 0, \frac{\partial S(x,y)}{\partial b_1(x,y)} = 0, \frac{\partial S(x,y)}{\partial c_1(x,y)} = 0. \quad (10)$$

From Eq. (10) we can obtain that (the spatial coordinates x, y have been omitted for notation brevity)

$$\begin{bmatrix} a_1 \\ b_1 \\ c_1 \end{bmatrix} = \begin{bmatrix} N & \sum_{n=1}^N \frac{B_n}{B_1} \cos \delta_n & \sum_{n=1}^N \frac{B_n}{B_1} \sin \delta_n \\ \sum_{n=1}^N \frac{B_n}{B_1} \cos \delta_n & \sum_{n=1}^N \frac{B_n^2}{B_1^2} \cos^2 \delta_n & \sum_{n=1}^N \frac{B_n^2}{B_1^2} \cos \delta_n \sin \delta_n \\ \sum_{n=1}^N \frac{B_n}{B_1} \sin \delta_n & \sum_{n=1}^N \frac{B_n^2}{B_1^2} \sin \delta_n \cos \delta_n & \sum_{n=1}^N \frac{B_n^2}{B_1^2} \sin^2 \delta_n \end{bmatrix}^{-1} \begin{bmatrix} \sum_{n=1}^N I_n^t - A_n + A_1 \\ \sum_{n=1}^N (I_n^t - A_n + A_1) \frac{B_n}{B_1} \cos \delta_n \\ \sum_{n=1}^N (I_n^t - A_n + A_1) \frac{B_n}{B_1} \sin \delta_n \end{bmatrix}. \quad (11)$$

From Eq. (11), the unknowns ($a_1(x,y)$, $b_1(x,y)$, and $c_1(x,y)$) can be solved. Then $A(x,y)$, $B(x,y)$, and $\Phi(x,y)$ can be determined as

$$A(x,y) = a_1(x,y), \quad (12)$$

$$B(x,y) = \sqrt{(c_1(x,y))^2 + (b_1(x,y))^2}, \quad (13)$$

$$\begin{aligned} \Phi(x,y) &= \varphi(x,y) + u_c x + v_c y \\ &= \tan^{-1}(-c_1(x,y)/b_1(x,y)), \end{aligned} \quad (14)$$

and $\partial\varphi(x,y)/\partial y$ will be more accurate, and the iteration will converge faster than that of without fitting.

C. Iterative Algorithm Determination of the Phase Shifts

Using the universal phase-shifting algorithm, phase distribution can be extracted if the phase shifts are known. If phase distribution is known, the average phase shifts of the entire pixels can be determined in a similar method but an inverse way. In the inverse algorithm, we defined another set of variables for the n th frame as $b'_n = \cos(\theta_n)$ and $c'_n = -\sin(\theta_n)$, where θ_n denotes the relative average phase shift ($\theta_1 = 0$, $\theta_2 = u_c$, $\theta_3 = v_c$, and $\theta_4 = u_c + v_c$). Thus Eqs. (4)–(7) are rewritten as

$$I_n^t(x,y) - A_n(x,y) = b'_n B_n(x,y) \cos[\Phi_n(x,y)] + c'_n B_n(x,y) \sin \Phi_n(x,y), \quad (15)$$

where $\Phi_1(x,y) = \Phi(x,y)$, $\Phi_2(x,y) = \Phi(x,y) + \partial\varphi(x,y)/\partial x$, $\Phi_3(x,y) = \Phi(x,y) + \partial\varphi(x,y)/\partial y$, and $\Phi_4(x,y) = \Phi(x,y) + \partial\varphi(x,y)/\partial x + \partial\varphi(x,y)/\partial y$. If $A_n(x,y)$, $B_n(x,y)$, and $\Phi_n(x,y)$ are known (obtained as step B), there are $2N$ unknowns and XYN equations, where the X and Y denote the number of pixels along the x and y axis, respectively. Therefore, the unknowns can be solved again by utilizing the over-determined least-squares method in the same way as step B (the spatial coordinates x, y have been omitted):

$$\begin{bmatrix} b'_n \\ c'_n \end{bmatrix} = \begin{bmatrix} \sum_{x=1}^X \sum_{y=1}^Y B_n^2 \cos^2 \Phi_n & \sum_{x=1}^X \sum_{y=1}^Y B_n^2 \sin \Phi_n \cos \Phi_n \\ \sum_{x=1}^X \sum_{y=1}^Y B_n^2 \sin \Phi \cos \Phi_n & \sum_{x=1}^X \sum_{y=1}^Y B_n^2 \sin^2 \Phi_n \end{bmatrix}^{-1} \begin{bmatrix} \sum_{x=1}^X \sum_{y=1}^Y (I_n^t - A_n) B_n \cos \Phi_n \\ \sum_{x=1}^X \sum_{y=1}^Y (I_n^t - A_n) B_n \sin \Phi_n \end{bmatrix}. \quad (16)$$

from which the linear carrier phase $u_c x + v_c y$ is easily removed to get $\varphi(x,y)$ by a subtraction operation after unwrapping $\Phi(x,y)$. Because of the errors of local phase shifts in the early iterations, the obtained $A(x,y)$, $B(x,y)$, and $\varphi(x,y)$ will be noisy. Thus we can reduce the noise by Zernike polynomial fitting [10] and estimate A_n , B_n , $\partial\varphi(x,y)/\partial x$, and $\partial\varphi(x,y)/\partial y$ from fitted $A(x,y)$, $B(x,y)$, and $\varphi(x,y)$, respectively. Then we insert A_n , B_n , $\partial\varphi(x,y)/\partial x$, $\partial\varphi(x,y)/\partial y$, and the unmodified $\Phi(x,y)$ into step C. With the Zernike polynomial fitting, the estimation of A_n , B_n , $\partial\varphi(x,y)/\partial x$,

Then the average phase shift can be determined from

$$\bar{\theta}_n = \tan^{-1}(-c'_n/b'_n). \quad (17)$$

Thus we can calculate the local phase shifts as $\theta_1(x,y) = \theta_1$, $\theta_2(x,y) = \theta_2 + \partial\varphi(x,y)/\partial x$, $\theta_3(x,y) = \theta_3 + \partial\varphi(x,y)/\partial y$, and $\theta_4(x,y) = \theta_4 + \partial\varphi(x,y)/\partial x + \partial\varphi(x,y)/\partial y$. Then we substitute $\theta_n(x,y)$ ($n = 1, 2, 3, 4$) into step B in next iteration circle.

D. Iterative Strategy for the Iterative Algorithm

The proposed algorithm first transforms the spatial carrier interferogram into four temporal phase-shifting interferograms and then utilizes least-squares iteration to calculate the phase distribution. During the iterations, there are three steps in each iteration cycle: step B is calculating $\Phi(x,y)$ based on $A(x,y)$ and $B(x,y)$ obtained in step B and $\theta_n(x,y)$ obtained in step C of the previous iteration cycle. Step C is determining θ_n from $\Phi(x,y)$, $A(x,y)$, and $B(x,y)$, which are all obtained in step B of this iteration cycle and then calculating $\theta_n(x,y)$. Step D is checking to see whether the results of the iteration satisfy the convergence criteria. It is θ_n that will converge, so the convergence criteria can be expressed as

$$|(\bar{\theta}_n^i - \bar{\theta}_1^i) - (\bar{\theta}_n^{i-1} - \bar{\theta}_1^{i-1})| < \epsilon, \quad (18)$$

where i represents the number of iterations and ϵ is the predefined threshold of accuracy.

The proposed algorithm contains the nonlinear iterative process. If the estimated initial $\theta_n(x,y)$ deviate from the actual values greatly, the obtained $\Phi(x,y)$ will have considerable errors. Thus $\partial\varphi(x,y)/\partial x$ and $\partial\varphi(x,y)/\partial y$ may produce large errors that make $\theta_n(x,y)$ deviate from the actual values further and result in instability in the iteration. Therefore, we first ignore the effects of $\partial\varphi(x,y)/\partial x$ and $\partial\varphi(x,y)/\partial y$ by setting $\Phi_n(x,y) = \Phi(x,y)$ and $\theta_n(x,y) = \theta_n$ during the iteration. After a few iterations until Eq. (18) meets a given accuracy, e.g., $\epsilon = 0.001$, the obtained $\Phi(x,y)$ and $\theta_n(x,y)$ will approximate the actual values. Then we substitute $\Phi(x,y)$ or $\theta_n(x,y)$ into the proposed iterative algorithm. The iteration will not stop until the criteria are met (e.g., $\epsilon = 10^{-4}$). Finally, $\Phi(x,y)$ and $\theta_n(x,y)$ in every pixel are updated and determined after iterations.

3. Numerical Simulations and Discussions

Since the exact expression of an actual object surface is hard to know due to many practical factors, a series of computer simulations have been carried out to verify the effectiveness of the proposed algorithm. To check its accuracy, we define the spatial carrier interferogram with a resolution of 128×128 pixels as

$$\begin{aligned} I(x,y) = & 130 \exp[-r_a(x^2 + y^2)] \\ & + 120 \exp[-r_b(x^2 + y^2)] \cos[2\pi(x^2 + y^2)] \\ & + u_c x + v_c y + n(x,y), \end{aligned} \quad (19)$$

where $-1 \leq x \leq 1$, $-1 \leq y \leq 1$; r_a and r_b denote the distribution parameters of the background and the contrast, respectively; and $n(x,y)$ denotes additive Gaussian white noise with a mean of zero and variance σ^2 . The difference between the calculated phase and the defined phase is defined as the residual phase error of the algorithm, which is characterized by peak to valley (PV) and root mean square (RMS) [10]. The performance of the proposed iterative algorithm is analyzed based on extensive numerical simulations.

A. Influence of Background and Contrast Variations

In the traditional SCPS algorithm, it is assumed that the background and the contrast are constants over consecutive pixels. If this condition cannot be preserved ($r_a \neq 0$ or $r_b \neq 0$), considerable errors will occur. But the proposed iterative method mentioned above can compensate for these errors. In order to show the performance of compensation for the influence of background and contrast variations, we set the spatial carrier frequencies u_c and v_c as 0.74 rad per pixel, standard deviation $\sigma = 0.01$, and $r_a = r_b$. Figure 1 shows the residual phase errors of the iterative algorithm with and without compensation for the effects of background and contrast

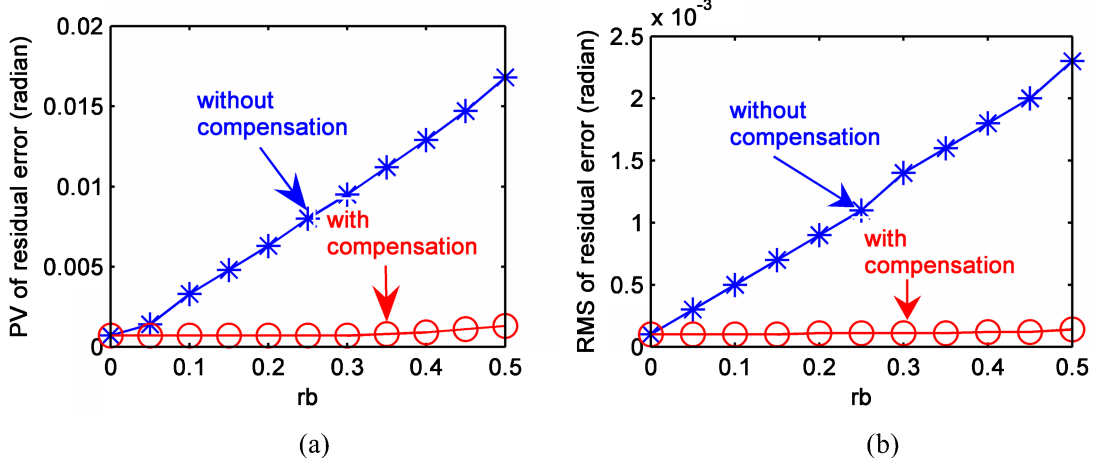


Fig. 1. (Color online) Residual phase error with and without compensation as a function of the parameter rb : (a) PV and (b) RMS.

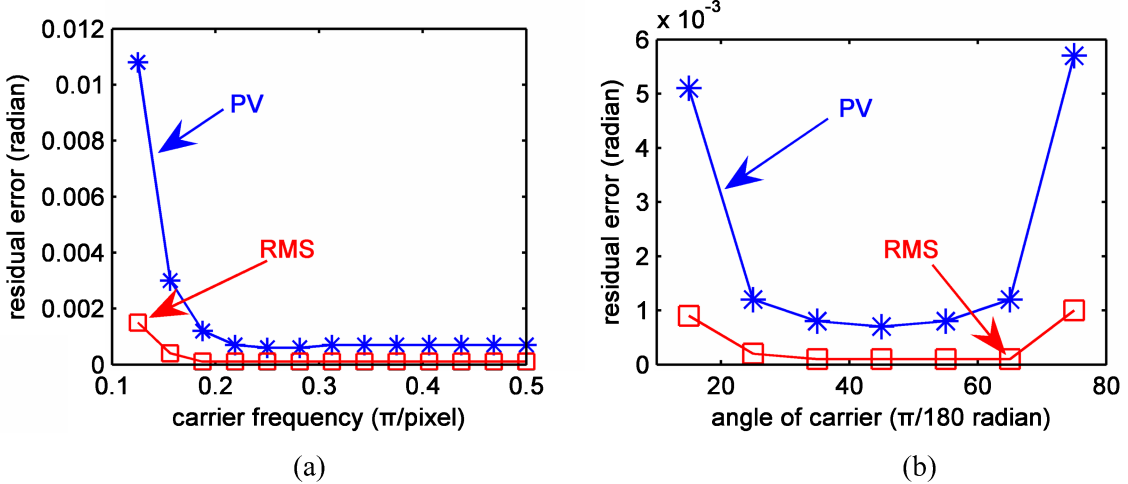


Fig. 2. (Color online) Residual phase errors as a function of the (a) magnitude and (b) direction of spatial carrier frequency.

variations. From Fig. 1, one can see that the PV and RMS of the residual phase error without compensation increase with increasing r_a and r_b . When dr_b increases from 0 to 0.5 (the intensity at the edge is about 37% of its maximum value), the PV and RMS of the residual phase error increase from 7×10^{-4} and 1×10^{-4} rad to 168×10^{-4} and 23×10^{-4} rad, respectively. After compensation, however, we reduce the residual phase error and keep it less than 13×10^{-4} (PV) and 1.4×10^{-4} (RMS) radian when $0 \leq r_b \leq 0.5$. Therefore, we can improve the accuracy of the iterative algorithm greatly by compensating for the effects of background and contrast variations.

B. Influence of Spatial Carrier Frequency

The traditional SCPS algorithm usually requires an appropriate spatial carrier frequency, $\pi/2$ or $2\pi/3$ rad per pixel for example. Although the proposed algorithm can calculate the local phase shifts and phase distribution simultaneously, it also needs some limits on the spatial carrier frequency; otherwise the iteration will not converge. Here we set $r_a = r_b = 0.5$ and $\sigma = 0.01$. We consider the influence of the magnitude of spatial carrier frequency by setting its direction as 45° ($u_c = v_c$) and then consider the influence of its direction by setting the magnitude as $\pi/2$ rad per pixel. Figure 2(a) presents the PV and RMS of the residual phase error as a function of the magnitude, and Fig. 2(b) presents the error as a function of the direction of spatial carrier frequency. The obtained results show that the residual phase error decreases as the magnitude of the spatial carrier increases from $\pi/8$ to $\pi/2$ rad per pixel and as the direction approaches 45° . It is also worth noticing that the PV of the residual phase error remains less than 0.002 rad when the magnitude and the direction of spatial carrier are in the range from $\pi/5$ to $\pi/2$ rad per pixel and 25° to 65° , respectively. When the magnitude of spatial carrier is less than $\pi/10$ or the direction ap-

proaches 0° or 90° , v_c or u_c will be close to zero. If v_c is close to zero, then in Eqs. (4)–(7), $I_2(x,y) \approx I_1(x,y)$ and $I_4(x,y) \approx I_3(x,y)$, thus four frames of interferograms become two independent interferograms. This will result in a big error in $\varphi(x,y)$ and slow convergence or instability in the iteration.

C. Influence of Random Noise

In all of the SCPS algorithms, the phase is computed from adjacent points, thus it is very sensitive to random noise. To analyze the influence of random noise, we set $r_a = r_b = 0.5$ and $u_c = v_c = 0.74$ rad per pixel. Figure 3 presents the PV and RMS of the residual phase error of our algorithm as a function of σ . The figure shows that the residual phase error increases linearly as σ increases from 0.01 to 0.9. If we set $\sigma = 1$, then the maximum noise gray level is about 7 and the ratio of signal to noise is about 82. For our algorithm, the PV and RMS of the residual phase error are 0.0502 and 0.04 rad, respectively. If we take four measurements and calculate the average of the phase result, then the residual phase error is reduced to 0.0243 (PV) and 0.02

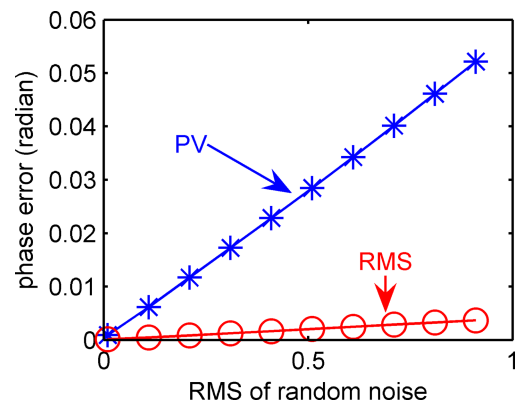


Fig. 3. (Color online) Residual phase errors as a function of the RMS of random noise.

(RMS) radian. We also find that the residual phase error is reduced by \sqrt{N} times if N measurements are taken and averaged. On the other hand, if a traditional four-bucket algorithm (temporal phase-shifting algorithm) is used to extract the phase from four interferograms with $\sigma = 1$ and phase step exactly equal to $\pi/2$, its residual phase error is 0.0085 (PV) and 0.0010 (RMS). Although the temporal phase-shifting algorithm exhibits higher precision, it needs four interferograms with accurate phase step; otherwise, a big error will occur.

D. Comparison with Another Spatial Phase-Shifting Algorithm

To compare the proposed method with Guo's method [7], common conditions are set ($u_c = 0.84$ rad per pixel, $v_c = 0.74$ rad per pixel, $r_a = r_b = 0.5$, and $\sigma = 0.01$). The spatial carrier fringe pattern is shown in Fig. 4(a). After 10 iteration circles of the proposed algorithm, the local phase shifts along the y axis and the phase distribution are calculated and shown in Figs. 4(b) and 4(d), respectively, the residual phase errors of which are shown in Figs. 4(c) and

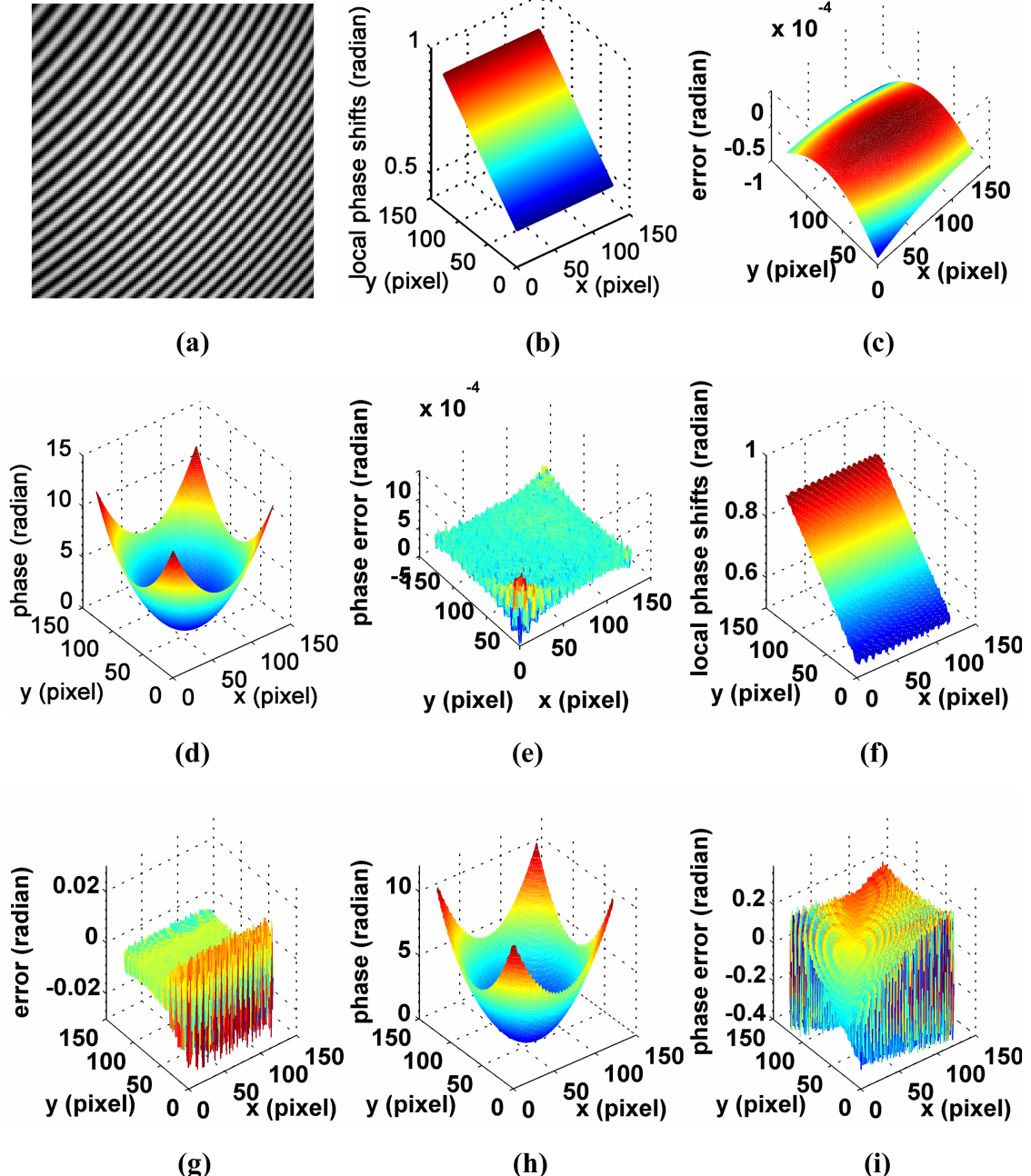


Fig. 4. (Color online) Simulation results: (a) carrier fringe, (b) local phase shifts along the y axis, (d) phase distribution obtained by the proposed method, and (c), (e) residual phase errors corresponding to (b), (d), respectively. (f) Local phase shifts along the y axis, (h) phase distribution obtained by Guo's method, and (g), (i) residual phase errors corresponding to (f), (h), respectively.

4(e), respectively. Figures 4(f)–4(i) present the corresponding results, which are calculated by Guo's method. Comparing Figs. 4(b)–4(e) with Figs. 4(f)–4(i), we find that our method presents more accurate local phase shifts and phase distribution than Guo's method. The reason is that our method contains an iterative procedure and compensates for the effects of the variations of phase shifts between pixels and the variations of background and contrast.

4. Experimental Work

For further verification of the performance of the algorithm, we apply it to the practical interferogram shown in Fig. 5(a). Then the proposed algorithm is used to extract the phase shown in Fig. 5(b), the PV and RMS of which are 0.6938 and 0.1236λ (here λ means the wavelength used in our experiment). Figure 5(c) presents the phase calculated by traditional five-point SCPS algorithm [11], and the PV and RMS of that calculation are 1.1651 and 0.1561λ , respectively. Meanwhile, the test surface is also measured by Zygo's interferometer with a vibration-isolating platform and a calibrated piezoelectric actuator device (PZT). The phase is extracted by Zygo's phase-shifting interferometry (PSI) algorithm and shown in Fig. 5(d), the PV and RMS of which are 0.7519 and 0.1295λ , respectively. Evidently, it can be concluded from Figs. 5(b)–5(d) that the phase distributions obtained by our algorithm and Zygo's PSI algorithm are almost the same except the edge of the interferogram, and the difference between them is less than 0.06 (PV) and 0.006 (RMS) λ . However, the difference between the phases obtained by traditional five-point SCPS algorithm and Zygo's PSI

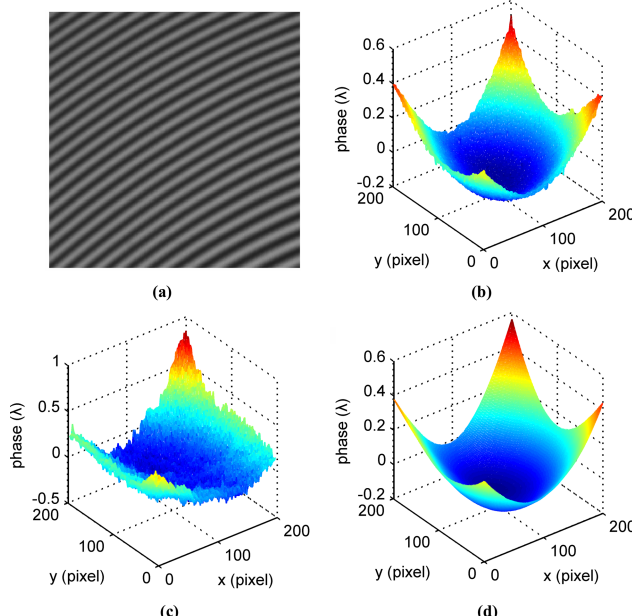


Fig. 5. (Color online) Experimental results: (a) interferogram with spatial carrier frequency, (b) phase map obtained by the proposed method, (c) phase map obtained by the five-point SCPS method, and (d) phase map obtained by Zygo's PSI method.

algorithm is more than 0.4 (PV) and 0.02 (RMS) λ . Therefore, the proposed method is advantageous over the five-point SCPS algorithm.

5. Conclusion

To conclude, we have proposed a new iterative algorithm to extract phase distribution from a single interferogram with spatial carrier. The algorithm divides the spatial carrier interferogram into four randomly phase-shifted interferograms and obtains the phase distribution and the phase shifts by a least-squares iterative procedure. To improve the accuracy of the iterative algorithm, the local phase shifts of the phase-shifted interferograms are obtained by compensating for the errors caused by the variations of phase shifts between pixels and the variations of background and contrast. When the intensity at the edge is about 37% of its maximum value, our method reduces the PV and RMS of the residual phase error from 168×10^{-4} and 23×10^{-4} rad to 13×10^{-4} and 1.4×10^{-4} rad, respectively. Numerical simulations show that the residual phase error decreases as the magnitude of the spatial carrier increases from $\pi/8$ to $\pi/2$ rad per pixel and as the direction of spatial carrier approaches 45°. Simulations and experiments demonstrate that the proposed algorithm is valid and exhibits higher precision than Guo's method and the traditional five-point algorithm. Although the temporal phase-shifting algorithm exhibits higher precision, the proposed algorithm can improve accuracy by taking the average of many measurements. Furthermore, only one single spatial carrier interferogram is needed, so the proposed method works well with a large aperture interferometer, especially for real-time and dynamic measurements in an environment with low frequency and high amplitude vibration. With the present method, costly and accurate phase-shifting devices are no longer required for steady-state measurement.

References

1. K. Creath, "Temporal phase measurement methods," in *Interferogram Analysis*, D. Robinson and G. Reid, eds. (IOP Publishing, 1993), pp. 95–140.
2. M. Takeda, H. Ina, and S. Kobayashi, "Fourier-transform method of fringe-pattern analysis for computer-based topography and interferometry," *J. Opt. Soc. Am.* **72**, 156–160 (1982).
3. M. Kujawinska and J. Wójciak, "Spatial-carrier phase-shifting technique of fringe pattern analysis," *Proc. SPIE* **1508**, 61–67 (1991).
4. P. H. Chan and P. J. Bryanston-Cross, "Spatial phase stepping method of fringe-pattern analysis," *Opt. Lasers Eng.* **23**, 343–354 (1995).
5. M. Pirga and M. Kujawinska, "Two directional spatial-carrier phase-shifting method for analysis of crossed and closed fringe patterns," *Opt. Eng.* **34**, 2459–2466 (1995).
6. M. Servin and F. J. Cuevas, "A novel technique for spatial phase-shifting interferometry," *J. Mod. Opt.* **42**, 1853–1862 (1995).
7. H. Guo, Q. Yang, and M. Chen, "Local frequency estimation for the fringe pattern with a spatial carrier: principle and applications," *Appl. Opt.* **46**, 1057–1065 (2007).

8. A. Styk and K. Patorski, "Analysis of systematic errors in spatial carrier phase-shifting applied to interferogram intensity contrast determination," *Appl. Opt.* **46**, 4613–4624 (2007).
9. Z. Wang and B. Han, "Advanced iterative algorithm for phase extraction of randomly phase-shifted interferograms," *Opt. Lett.* **29**, 1671–1673 (2004).
10. D. Malacara and S. L. DeVore, "Optical interferogram evaluation and wavefront fitting," in *Optical Shop Testing*, D. Malacara, ed. (Wiley Interscience, 1992).
11. M. Pirga and M. Kujawinska, "Errors in two-dimensional spatial-carrier phase-shifting method for closed fringe pattern analysis," *Proc. SPIE* **2860**, 72–83 (1996).